

http://pubs.acs.org/journal/aesccq Article

Is Ice Formation by Sea Spray Particles at Cirrus Temperatures Controlled by Crystalline Salts?

Ryan J. Patnaude,* Russell J. Perkins, Sonia M. Kreidenweis, and Paul J. DeMott



Cite This: https://doi.org/10.1021/acsearthspacechem.1c00228



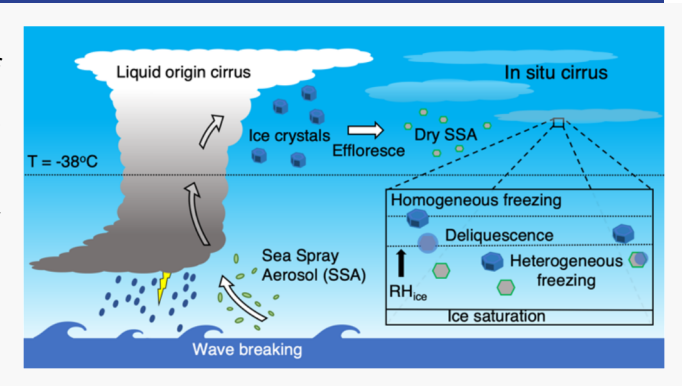
ACCESS

III Metrics & More

Article Recommendations

Supporting Information

ABSTRACT: The ice nucleating ability of sea spray aerosol (SSA) particles has been explored in recent years due to the abundance of SSAs in the atmosphere. The role of SSAs in ice nucleation extends to cirrus clouds, due to processes that loft SSAs to the upper troposphere. This is of special relevance because of the frequent occurrence of cirrus in the atmosphere, their role in the Earth's radiative balance, and uncertainties regarding how aerosols may affect their formation and evolution. In this study, a continuous flow diffusion chamber (CFDC) is used to investigate the ice nucleating ability of size-selected particle distributions of SSAs and its primary constituent sodium chloride (NaCl) at temperatures <235 K. Results show that, above ~220 K, the majority of NaCl and SSA particles fully deliquesce and freeze via homogeneous



nucleation at or below water relative humidities, RH_w , of ~95%. However, below 220 K, the onset RH_w of freezing for NaCl and SSA particles is much lower, at ~75%, where strong heterogeneous freezing of 10% of the aerosol population occurs. Similar heterogeneous freezing behavior for NaCl and SSA particles, occurring near their predicted deliquescence RH_w , points toward SSA freezing at the lowest temperatures being controlled by the crystalline salts. Finally, the calculations of ice nucleation active surface site densities show that particle size does not dictate the efficiency of freezing for NaCl and SSA particles. These results indicate SSAs as a potentially significant source of ice nucleating particles at cirrus temperatures, with the ability to contribute to cirrus-mediated climate impacts if sea spray emission and transport scenarios change in the future.

KEYWORDS: cirrus clouds, ice nucleation, sea spray aerosols, sodium chloride, pore-condensation freezing, homogeneous freezing, heterogeneous freezing

1. INTRODUCTION

Cirrus clouds are ubiquitous and play a significant role in global radiative balance. 1-3 Composed entirely of ice at temperatures <235 K, their formation in the atmosphere is controlled by upper tropospheric dynamical processes and the interplay between two basic ice nucleation pathways, homogeneous freezing and heterogeneous ice nucleation, which determines the size and number of ice crystals, and consequently can determine the sign of the radiative effect of the clouds.^{4,5} The homogeneous freezing of condensed water is the process that will ultimately occur for the dissolved solute particles that constitute the major aerosol population capable of acting as cloud condensation nuclei (CCN), unless heterogeneous nucleation on a more specialized subset of aerosols intervenes to glaciate clouds before the relative humidity (RH) and solute dilution conditions required for homogeneous freezing can occur^{6,7} as discussed further below. Heterogeneous freezing requires an ice nucleating particle (INP) that catalyzes a freezing event by lowering the required energy in the activation process. Depending on environmental factors such as temperature and relative humidity, heterogeneous freezing may proceed via several different nucleation modes. First, immersion freezing is described by an INP becoming "immersed" in an aqueous solution or water droplet, with the presence of the particle surface initiating freezing. Often included in the immersion mode, as experimentally indistinguishable, condensation freezing describes the simultaneous uptake of liquid water on an INP and freezing. In contrast, deposition nucleation does not require any liquid water phase formation, instead forming ice directly from the supersaturated vapor onto an INP. However, it has been posited that this mechanism actually proceeds via a pathway of pore condensation freezing (PCF) in cavities on the surface of an INP. 10–12

Special Issue: Mario Molina Memorial

Received: June 25, 2021 Revised: August 2, 2021 Accepted: August 5, 2021



The homogeneous freezing of nearly pure water in the form of dilute cloud droplets depends on droplet size (volume) and temperature but typically occurs by 235 K as clouds cool, and this temperature roughly brackets the highest temperature end of cirrus cloud formation. At lower temperatures solution droplets (unactivated CCN), formed when the RH exceeds that required for deliquescence, will freeze according to the solution water activity and the ambient temperature. 13 As a consequence, relatively high ice supersaturation (SSi, equal to relative humidity with respect to ice (RH_i) minus 100%) must be achieved for homogeneous freezing to occur. 14 Heterogeneous nucleation via condensation/immersion freezing can occur across the full range of tropospheric temperatures, primarily within dilute cloud droplets at higher temperatures characteristic of mixed phase clouds but progressively within more concentrated solution droplets at the lower temperatures that are characteristic of cirrus clouds. Whereas a freezing temperature can be stated to characterize where a particular ice nucleating particle type begins to freeze strongly via immersion freezing in dilute cloud droplets at mixed phase cloud temperatures, a water or ice relative humidity condition may be used to characterize the conditions for heterogeneous cirrus nucleation, reflecting solute compositional impacts on freezing. 15,16

During cirrus cloud formation, both heterogeneous and homogeneous nucleation may be active or the former may dominate. The active nucleation mechanisms are determined by the number of INPs, their freezing onset characteristics, and the maximum relative humidity achieved, the latter of which depends on the strength and persistence of vertical motions that increase supersaturation against water vapor consumption by growing ice crystals. ¹⁷⁻²⁰ Homogeneous freezing will ensue when the RH_i exceeds the homogeneous freezing threshold (140%-150%, depending on temperature).²¹ Recent studies have attempted to group cirrus clouds in two categories, liquid origin and in situ, that are based on their dominant formation mechanism and the strength of vertical motions. 22-24 Liquid origin cirrus are driven by deep convection, including contributions of heterogeneously frozen drops from the mixed phase regime and homogeneously frozen droplets that persist to cirrus levels, while in situ origin cirrus clouds form entirely below 235 K via homogeneous and heterogeneous nucleation. Liquid origin cirrus clouds generally contain high ice water content and ice crystal number concentrations, with the opposite for clouds of in situ origin. 23 Both cirrus origins may occur under either fast or slow updraft conditions that largely determine the nucleation mechanism, where the former scenario likely leads to a dominance of homogeneous freezing and the latter proceeds via heterogeneous nucleation (albeit still debated in the literature). Meteorological scenarios where in situ cirrus may occur are synoptic scale systems (slow updraft) and gravity waves induced by jet streams, mesoscale convective systems, and anvils (fast updrafts). 22,23 One study inferred that cirrus have predominantly heterogeneous nucleation origins based on the ice residuals (IRs) that indicated the presence of INPs and the lower saturation requirement for nucleation in subtropical and tropical cirrus clouds.²⁵ However, the dominant process of cirrus formation remains more broadly unresolved⁶ and likely varies depending on the particular aerosol and cloud dynamical scenario.

Despite significant efforts, the role of specific types of aerosol particles in the formation of cirrus clouds remains highly uncertain. ²⁶ In limited and specialized in situ

observations, particles such as mineral dust and metallic particles have been noted to make up the largest fraction of IRs in cirrus clouds. 25,27,28 Black carbon and isoprene-derived secondary organic aerosols (SOAs) are frequently observed in the upper troposphere.^{29–31} While black carbon is known to contribute significantly to IRs in contrails, observations mostly suggest that these particle types do not contribute strongly as INPs in cirrus clouds, even though pathways for such action involving the processing of larger aggregates have recently been revealed.³² Certain SOAs have been observed to freeze heterogeneously with low active fractions,³³ but most SOAs are expected to freeze via the homogeneous pathway. Sea spray aerosol (SSA) particles also deserve attention in this regard due to their abundance in the atmosphere³⁴ and the fact that sea salt particles have been observed to make up a significant fraction of the IR in cirrus clouds over ocean regions, where deep convection lofts particles to the upper troposphere where they are detrained from the cloud itself and can persist at high altitudes. 25,28,35 While it has been assumed that the role of SSAs on impacting cirrus formation would most likely come about via their dominant composition as soluble species, 18 their phase states when lofted to the upper troposphere could present scenarios where their action as heterogeneous INPs should be considered. In the upper troposphere, SSA concentrations can range between 10^{-4} and 10^{-1} μ g m⁻³, on the basis of in situ and satellite observations. ^{36,37} In terms of relative abundance, SSAs are more scarce than sulfate particles, which have been reported to make up a large percentage of aerosols in the upper troposphere. However, only a very small fraction of sulfate particles freeze heterogeneously at these temperatures, ⁴⁰ and therefore, any heterogeneous freezing potential of SSAs could prove significant. For example, in a case study of Hurricane Nora, the authors speculated that marine aerosols generated and lofted in the deep convective core seeded cirrus clouds over a spatially and temporally vast region. 41 Thus, understanding the ice nucleating mode of SSAs at cirrus temperatures deserves further attention.

SSAs are generated during wave breaking by the bursting of small film and jet-drop bubbles at the sea surface microlayer. 42,43 Their composition may broadly include organic materials such as lipids, amino acids, saccharides, phytoplankton cell fragments, and inorganic sea salts. 44,45 While dissolved, surface active, and particulate organic matter in SSAs is known to serve as a source of low concentrations of immersion freezing INPs in a mixed-phase cloud regime $(>-38 \, ^{\circ}\text{C})$, ⁴⁶ the propensity of these to freeze at cirrus temperatures still remains uncertain, especially since ice nucleation modes there may be more varied. A number of studies have attempted to elucidate the heterogeneous nucleation ability of SSA in cirrus conditions using commercially available synthetic seawater products $^{47-51}$ and produced inconsistent results on whether the organic material enhanced or suppressed nucleation. However, using Prochlorococcus as a source of organic matter to mimic natural marine aerosols, polysaccharides and proteins were found to potentially enhance the efficiency of SSA nucleation, whereas lipids were ineffective INPs. 48 Of further consideration at cirrus temperatures, some previous studies have shown that aqueous particles containing organic material may transition into a highly viscous semisolid or solid glassy state. 52-55 One study using citric acid tested the role glassy aerosols may play in ice nucleation and found that, below 212 K, a fraction of glassy aerosols can freeze at relative humidities below those at which homogeneous nucleation would be

expected.⁵⁶ The ability of glassy aerosols to nucleate ice has largely been determined by the glass transition temperature and hygroscopicity, both of which can be affected by chemical aging and size of the particles.⁵⁷ Despite this freezing behavior of glassy aerosol, it is still assumed that they would freeze at low fractions similar to secondary organic aerosols.³³

In the past decade, a number of studies have also investigated the inorganic components of SSA for their role in ice nucleation. 47–50,58–60 As the major component of natural seawater, sodium chloride (NaCl) has frequently been used as a proxy for sea spray aerosol. 61 The pathway of ice nucleation for NaCl has been found to be largely determined by the phase state of the salt particles, where the mode of freezing is dependent upon the competition between deliquescence and heterogeneous freezing. 42,44,52 One study using the AIDA cloud chamber showed that both anhydrous NaCl and NaCl dihydrate particles that were fully deliquesced froze via homogeneous freezing above 225 K when exposed to a high SS_i. However, near their deliquescence point and below about 225 K, NaCl particles formed an internally mixed liquid-solid phase with solid crystalline remnants and froze via the immersion mode.⁴⁹ NaCl particles below their deliquescence relative humidities (DRHs) remained solid and were reported to freeze via the deposition mode. 59,60 These prior studies used different particles sizes (\sim 0.7-10 μ m), and it is unclear how size affected the heterogeneous nucleation of NaCl particles. Finally, effloresced aqueous NaCl at cirrus temperatures can form hydrated salts that have been reported to act as heterogeneous INPs. 58,59 One study using air mass trajectory analysis showed that hydrated salt particles may be present 40%-80% of the time at temperatures between 180 and 220 K when lofted from the boundary layer and detrained in deep convective anvils. 59 The extent to which the organic components or non-NaCl salt contents affect the ice nucleating ability of natural seawater has received only limited attention in the current literature and remains uncertain.

In the study presented herein, the ice nucleating ability at temperatures below 235 K of particles generated from natural seawater is examined. We probe the freezing behaviors of lab-generated aerosols using a continuous flow diffusion chamber (CFDC)^{16,62,63} that has been modified to reach temperatures below 200 K. We compare the ice nucleation characteristics of natural seawater-derived particles to pure NaCl particles and explore whether particle size impacts ice nucleation efficiency. The experimental design and aerosol generation and characterization are discussed in Section 2. Results showing fractional freezing conditions for NaCl and natural seawater particles and the atmospheric implications are discussed in Sections 3 and 4, respectively.

2. METHODS

2.1. CFDC Setup. Ice nucleation experiments were conducted with a CFDC at Colorado State University (CSU) on the basis of previously described designs ^{16,63-65} modified to measure ice nucleation at temperatures from 240 to 190 K. The CFDC consists of two concentric cylinders, which are coated in a thin layer of ice. The inner and outer walls of the chamber are held at different temperatures, producing gradients in both temperatures and water partial pressure. This can be used to create relative humidity conditions above saturation with respect to either ice or water. Sheath air flow is inserted into the column, allowing sample flow to enter the column and remain in a narrow,

central lamina flow. Calculations are carried out to determine temperature and supersaturation conditions experienced by aerosol within the instrument. These calculations are based on those of Rogers in 1988⁶² but were modified to more accurately represent instrument geometry and prevent the breakdown of calculations at low temperatures and flow rates. A full derivation of the current calculations and discussion of measurement uncertainties can be found in the Supporting Information. Prior to nucleation experiments, the column is chilled to 246 K and filled temporarily with deionized water to produce the ice coating along the column walls.

Some modifications to the physical design and mode of operation were made to the low temperature CFDC as compared to its previous configuration. First, flow rates were reduced through the 1.51 m chamber (Figure 1), resulting in a

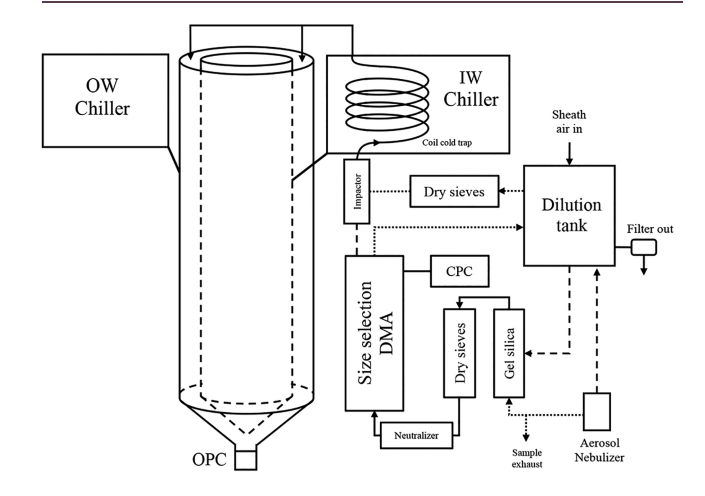


Figure 1. Diagram of the setup for SSA and NaCl generation, size selection, and flow configuration for CFDC experiments. Note, dashed and dotted lines indicate the pathway during experiments when selecting for 150 and 600 nm aerosols, respectively, and solid lines indicate the shared pathway for both aerosol sizes.

longer residence time of aerosols to promote activated ice crystal growth. The residence time is increased by operating at lower flow rates of 1 LPM_v sample flow and 4 LPM_v sheath flow (volumetric flows measured at column conditions not ambient) than have been used in the past, where typically a 10:1 sheath to sample flow ratio has been used. This additional residence time is helpful because ice crystal growth slows with decreasing temperature, as water partial pressures decrease for a given SS_i, and final aerosol size is used to distinguish between frozen and unfrozen aerosol, as discussed in Section 2.3. Additionally, the bottom section of the column was plumbed to allow for operation either as an evaporation section (constant temperature walls, RH_i ~ 100% or slightly above) or as an additional growth section (walls held at the same temperature throughout the chamber). Evaporation sections are useful in situations at >235 K where positive water supersaturations (SS_w, equal to RH_w - 100%) are required to activate water droplets prior to immersion freezing by a small subset of the particles. In that case, the evaporation section at a low SS; causes water droplets to evaporate toward liquid aerosol sizes while ice crystals continue to slowly grow, such that only ice crystals sustain sizes far exceeding aerosol sizes and are thus detected as nucleated particles. Under the low temperature conditions of this study, however, the growth region is held below water saturation, where particles achieve

at most haze sizes, so an evaporation section is not required. For all experiments described here, the bottom section of the column is used as additional growth section, allowing for extra residence time at growth conditions. This extra growth time allows for clearly distinguishing the nucleated ice crystal mode from the aerosol mode optically, as discussed later.

A second and minor change to the laboratory CFDC configuration is the use of two ultralow temperature circulating bath chillers (Thermo Scientific ULT-95) to control the fluid circulated to inner and outer walls of the chamber, extending the effective operating range beyond the ~211 K lower lamina temperature achieved in past studies. The bath fluid used is a low temperature, low viscosity, high thermal conductivity silicone oil (Syltherm XLT, Dow). This allows for lower temperature operation with very stable temperatures and negligible gradient across a given wall of the instrument.

Finally, the sample and sheath air drying systems were modified from standard desiccant drying systems to cold traps. For low temperature operation, standard desiccants such as silica gel and molecular sieves do not provide sufficient drying. Molecular sieves, for example, can dry ambient air to a RH of ~1%. At 25 °C, this corresponds to a vapor pressure of about 0.31 mbar. If this same air mass is cooled to -65 °C, this corresponds to a SS_w of ~3200%, which would prevent meaningful instrument operation. Although such instant cooling and high SSw are an extreme scenario, to avoid this problem, cold traps were installed in both the sheath and sample lines submerged in the cold wall chiller bath. These traps are simple coils of copper tubing, 3.4 and 2.2 m long for the sheath and sample traps, respectively. The bath is a few degrees colder than the cold inner wall of the instrument, which is always colder than the temperatures the aerosol experience within the instrument. The trap will force the RH to ice saturation at the trap temperature, which will always be a lower vapor pressure than ice saturation under aerosol conditions in the growth region of the instrument. Hence, all sample and sheath air entering the instrument will remain below ice saturation upon cooling. One additional consideration with this approach is that incoming sample air should be allowed to warm between the cold trap and introduction into the growth chamber to allow for the transport of residual water off the aerosol particles. Given the small mass of aerosol relative to air, the effect on RH of water evaporating from the aerosol is negligible.

2.2. Description of Aerosol Generation and Phase State. Aerosol measurements and size distributions were obtained using a combination of a differential mobility analyzer (DMA, TSI model 3071A), a condensation particle counter (CPC, TSI model 3010), and an aerodynamic particle sizer (APS, TSI model 3321). In this study, natural seawater (SW) collected from the Scripps Pier in La Jolla, CA was used for SSA generation. The seawater was stored in the dark and flown at room temperature to CSU. It was then filtered through a $0.22 \mu m$ sterile PES filter to sterilize the seawater to prevent any microbial growth and remove additional insoluble material such as dust and sand that may be present. Following filtration, it was again stored in the dark until use. For comparison, we used a 3.5% by weight NaCl (certified ACS, Fisher Chemical) solution prepared with deionized water to mimic the salt content of seawater. Aerosols were generated using a B&F Medical Aeromist Nebulizer and dried at room temperatures using a silica gel diffusion dryer followed by a molecular sieve dryer. Particles were then size selected at either 150 or 600 nm

using the DMA, operated with sheath(sample) flows of 10(2)and 4(1) LPM_v respectively. Aerosol concentrations were diluted to achieve concentrations in the range 100-500 cm⁻³, and depending on the aerosol size, the configuration of the dilution tank and DMA was rearranged to control aerosol flow into the DMA. For example, for 150 nm particles, the dilution tank was located upstream of the DMA, and the opposite was true for 600 nm (Figure 1). An additional molecular sieve dryer was required after the dilution tank for 600 nm particles as the sheath air contained small amounts of water vapor and would build up ice in the cold trap during experiments. Finally, particles size selected at 600 nm were passed through a 2.5 μ m aerodynamic impactor before entering the CFDC, in order to limit larger particles that would have made discerning small, activated ice crystals difficult at the slow growth rates present at cirrus temperatures.

Previous studies have shown that two crystalline structures can form via the efflorescence of NaCl, i.e., anhydrous NaCl and NaCl dihydrate (NaCl·2H₂O), where the former is the stable phase above ~273 K and the latter below ~273 K. 66 For this study, since NaCl particles are dried beyond their efflorescence RH of ~45% at room temperature, it is assumed the particles entering the CFDC have an anhydrous NaCl structure (see trajectory phase state diagram, Figure 2). Although the injection of the seed particles into the CFDC system occurred at temperatures below 273 K, dry NaCl particles remained below the eutectic and thus likely retained the anhydrous NaCl form, compared to scenarios where some aqueous particles that effloresced below 252 K formed NaCl·

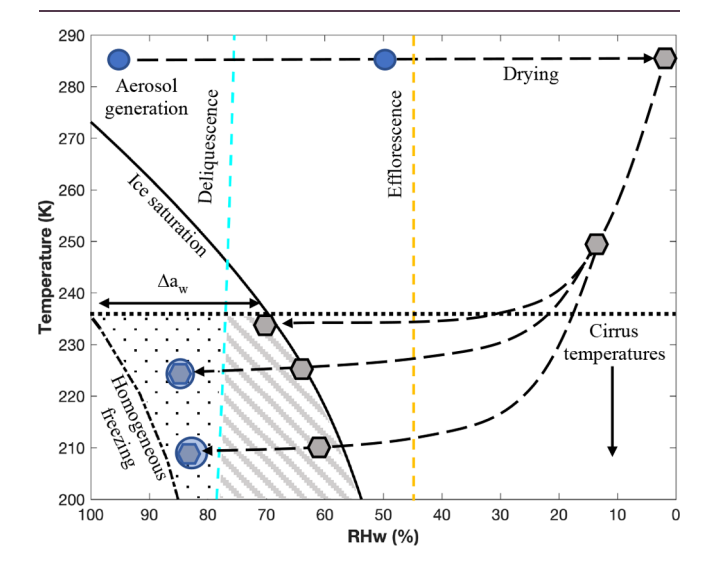


Figure 2. Expected trajectory and phase state of the NaCl and SSA particles for CFDC experiments. Cyan and orange dashed lines are the expected deliquescence and efflorescence lines, respectively, for NaCl on the basis of the parametrization of anhydrous NaCl and extrapolated to cirrus temperatures. The long dashed black line follows the path of aerosol particles as through drying, cooling, and CFDC scans at different temperatures. The blue circles represent aqueous NaCl and SSA solutions, gray hexagons represent effloresced aerosols, and the light blue circles with embedded hexagons represent deliquesced particles. Lines indicating ice saturation and predicted homogeneous freezing conditions are also denoted. The gray hatched region indicates ice supersaturated conditions with dry aerosols, and the dotted region represents conditions where aerosol particles experience ice supersaturated conditions and relative humidities that exceed their deliquescence point.

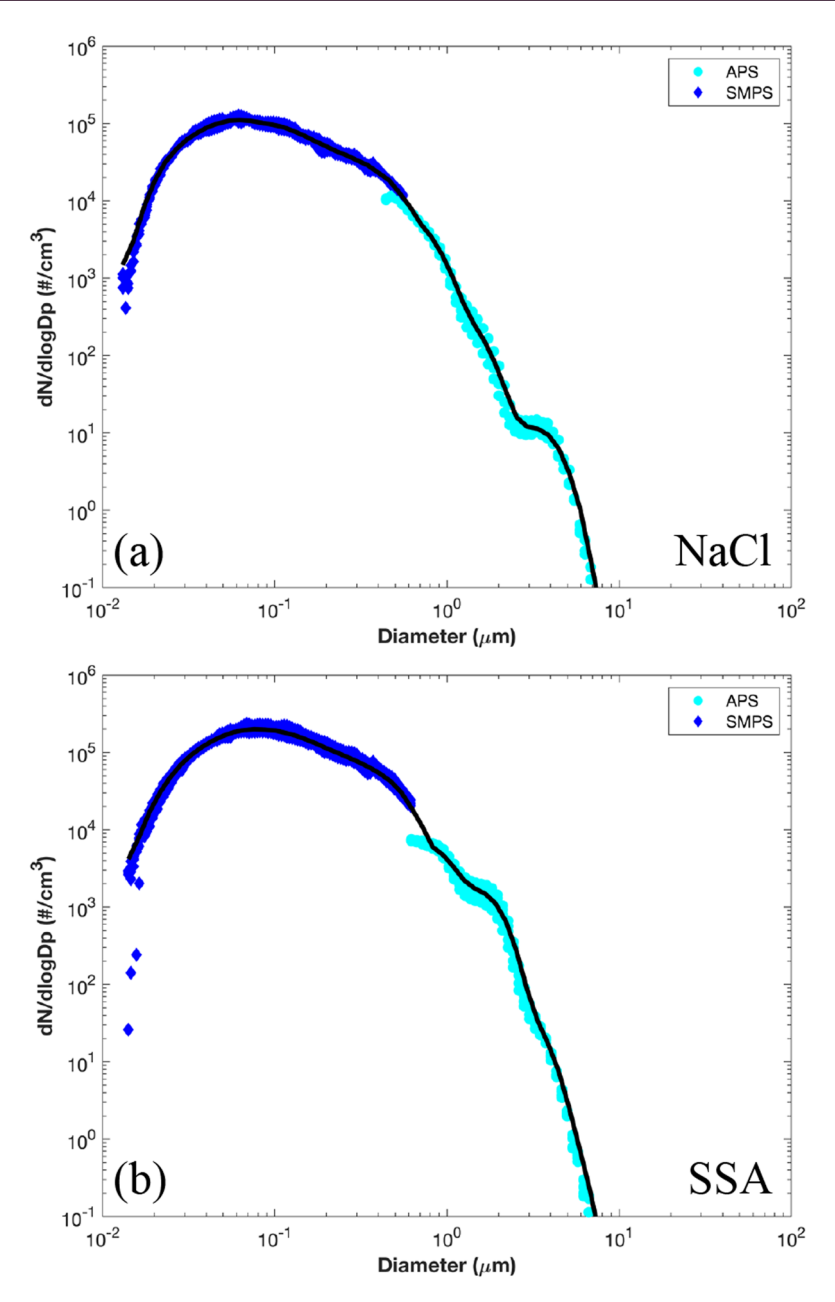


Figure 3. Combined particle size distributions for (a) NaCl and (b) SSA particles by combining measurements from a SMPS (blue diamonds) and an APS (cyan circles). The solid black line is the best fit from four measurement scans from the SMPS and APS.

2H₂O.⁵⁹ Therefore, we discounted the possibility that the experimental results reflected the sampling of NaCl·2H₂O in this study. The structure of the SSA particles is more complex to characterize at low temperatures. Although very low RHs are achieved during aerosol drying after generation and before introduction into the CFDC, prior work has demonstrated that it is likely that SSA particles retain liquid water, due to the presence of ions other than sodium and chloride and varying organic components. The range of organic mass fractions in submicron SSA particles may vary but previous studies generally show an increase with decreasing particle size. We assume the SSA particles in this study would exhibit similar characteristics but cannot rule out some differences due to varying generation methods. Additionally, it is possible for small amounts of other salts (i.e., magnesium

and calcium) in SSAs to precipitate prior to the NaCl contents. 70

Figure 3 shows the combined size distributions from the SMPS and APS for NaCl and SSA particles after drying but before size selection. The blue diamonds denote SMPS data with a measurement range of 12–615 nm, and cyan circles denote APS data with a measurement range of 520 nm–20 μ m. The black solid line represents the best fit line averaged for four separate scans from the SMPS and APS. APS measurements were converted to true diameter from aerodynamic diameter using eq 1:

$$D_{\rm t} = D_{\rm a} \sqrt{\frac{\chi}{\rho_{\rm p}}} \tag{1}$$

where $D_{\rm t}$ is the true diameter, $D_{\rm a}$ is the aerodynamic diameter, χ is the dynamic shape factor, and $\rho_{\rm p}$ is dry particle density. For

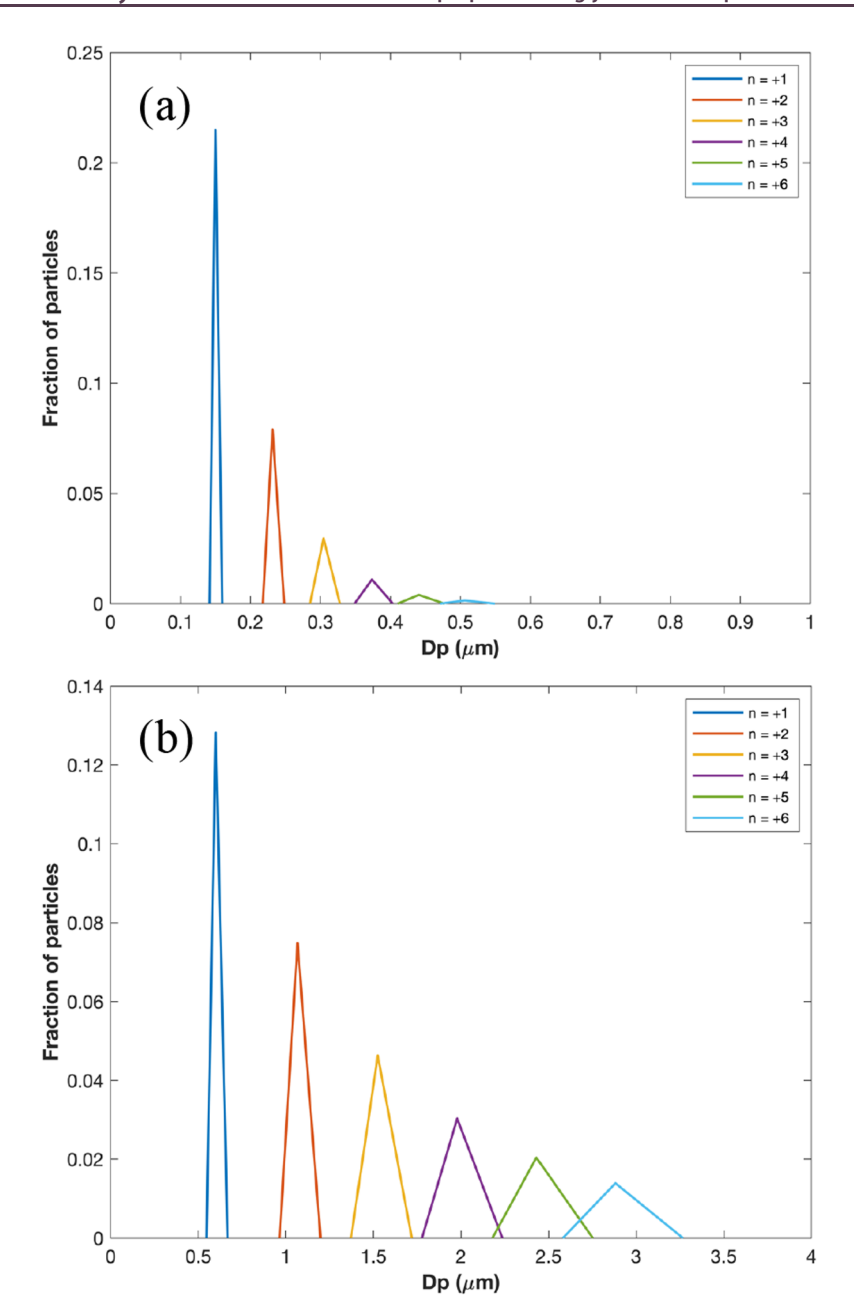


Figure 4. Fraction of particles represented by a given DMA multiplet, ranging from charges of +1 up to +6 for a monodisperse aerosol distribution of (a) 150 and (b) 600 nm particles.

dynamic shape factor, we used 1.08 and 1.05 for NaCl and SSA particles, respectively, 71 and estimated particle densities for SSAs and NaCl of 2.2 72 and 2.16 g m $^{-3}$, respectively. The resulting corrections shifted APS data toward slightly smaller sizes. In general, the distributions of both NaCl and SSA particles had peaks $\sim\!100$ nm. The SSA distribution indicated an increase in the number concentrations of particles <1 μ m of almost five times that obtained for NaCl and also showed a broader distribution of particles >1 μ m, consistent with previous studies using a similar method combining SMPS and APS data for SSAs. 73,74

Figure 4 shows the fraction of different sized particles predicted to be present after size selection at 150 and 600 nm with the DMA. For SSAs (NaCl), a +1 charge represents 74% (76%) of the sample after applying the fractional contributions of the monodisperse aerosol population for 150 nm and 86%

(92%) for 600 nm, on the basis of their respective size distributions. Larger, multiply charged particles were present in sufficient numbers so that we must consider their effects in the detection of frozen particles, as discussed below, and explicitly account for their contributions to aerosol surface area, as discussed in Section 3.

2.3. Ice Nucleation Detection. For the detection of ice, an optical particle counter (OPC) located immediately downstream of the CFDC column detects particle sizes. Aerosol particles that do not freeze or deliquesce will not change size appreciably. Frozen particles, however, will grow rapidly, only constrained by the rate of diffusional growth and residence time in the instrument. To distinguish between frozen and unfrozen particles, we introduced a size bin cutoff in OPC response. This size cutoff was determined by analyzing the distribution of seed particles from the OPC against the

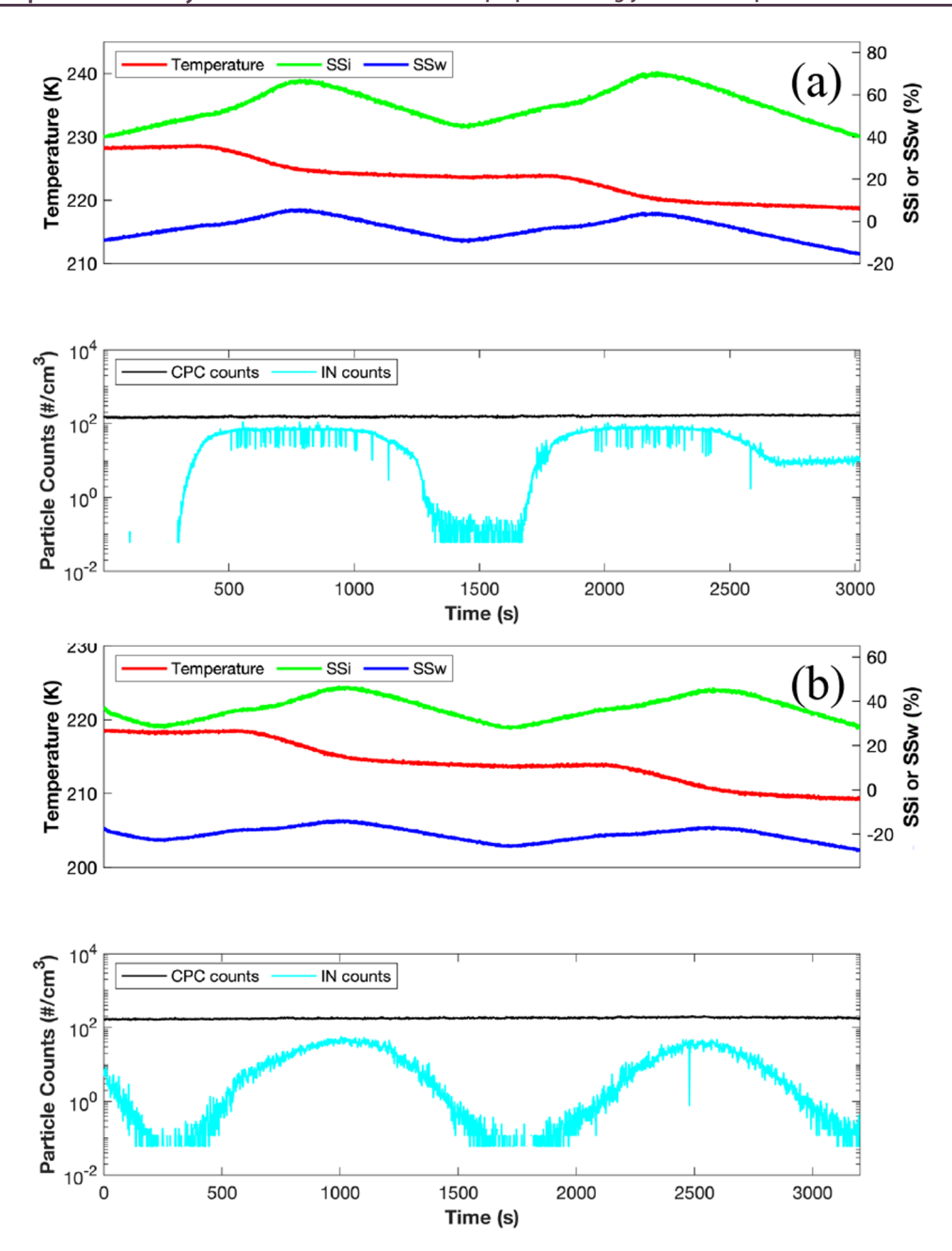


Figure 5. CFDC time series for NaCl experiments at (a) ~228 and 223 K and experiments at (b) ~218 and 214 K. The red line indicates temperature, and the blue and green lines indicate water and ice supersaturations, respectively. The black and cyan lines indicate the number of particles from the CPC and ice nucleating particles, respectively.

distribution of particles at conditions where a high frozen fraction was observed and is different for 150 and 600 nm particles but identical between temperatures. The size bin cutoff was chosen such that no ice nucleation was detected for NaCl samples at higher temperatures where ice nucleation is not expected to occur. This approach essentially accounts for the impacts of larger multiply charged particles passing through the DMA, ensuring that those large particles are not counted as frozen particles unless they have actually frozen.

3. RESULTS

For ice nucleation experiments, the procedure for the CFDC involves "scans" while sampling the aerosol stream, where RH_w and RH_i increase over time at a quasi-steady laminar

temperature, which is achieved by incrementally increasing the outer wall temperature $(T_{\rm OW})$ while holding the inner wall temperature $(T_{\rm IW})$ constant. Once a fraction of ice of 10% is reached, the $T_{\rm IW}$ is stepped down 5 K and the $T_{\rm OW}$ is decreased incrementally until the fraction of ice is <0.1%. The cycle is generally repeated 4–6 times until temperatures reach <220 K. For each aerosol type and size, two CFDC scans were conducted, one beginning at ~228 K and one at ~223 K, totaling eight experiments. The time series in Figure 5 represent scans for 150 nm NaCl particles at different temperatures producing different freezing results. For example, Figure 5a shows two subsequent CFDC scans that began at 228 and 223 K. In the first case, there was no ice formation until the SS_i reached nearly 50%, and there was a sudden

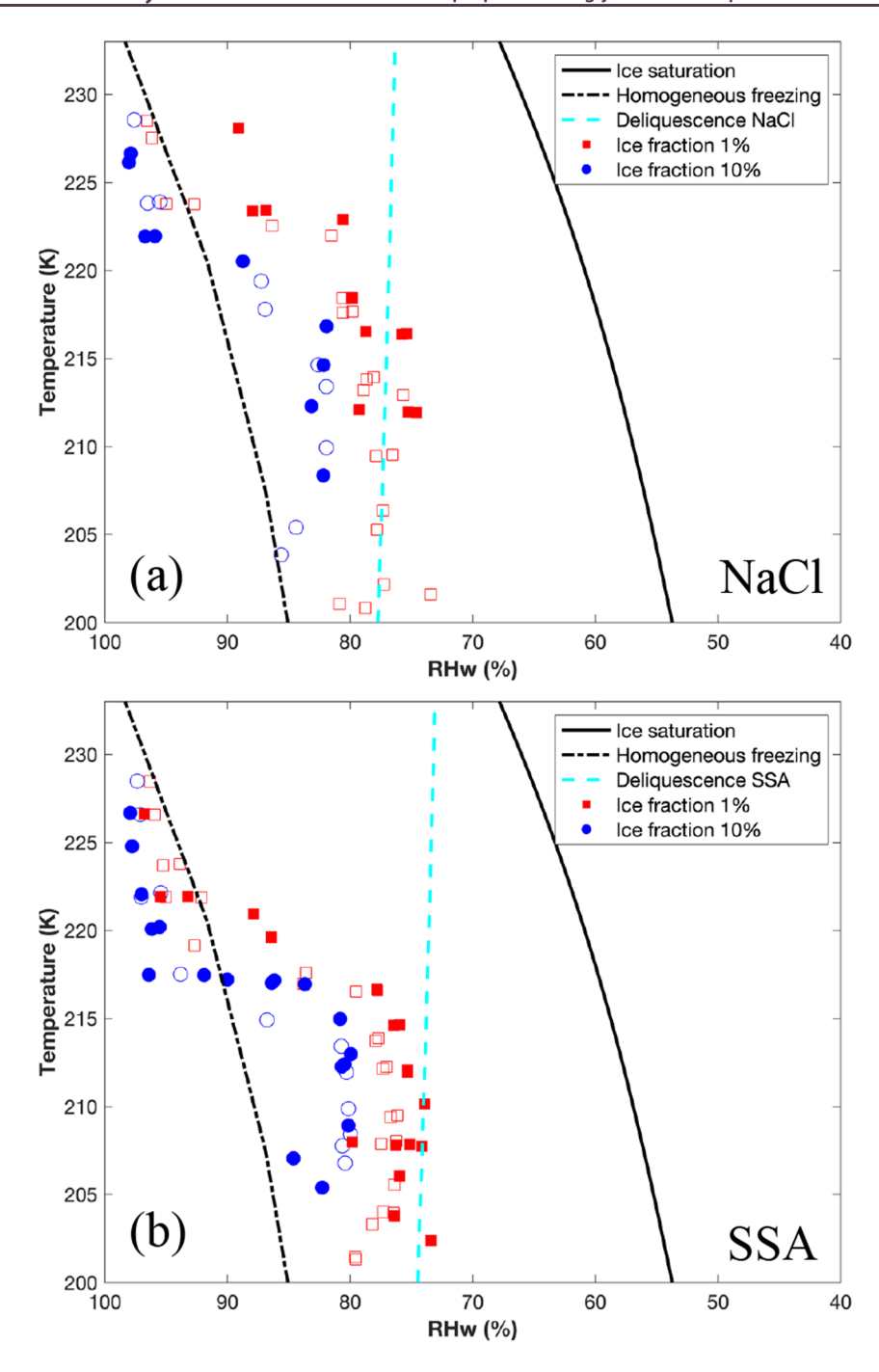


Figure 6. Ice fractions for (a) NaCl- and (b) SSA-generated particles. Blue and red markers denote 10% and 1% frozen fractions, respectively, where filled markers represent 600 nm particles and open markers for 150 nm particles. The dashed cyan line represents the predicted deliquescence for NaCl⁷⁰ and was lowered by 4% RH_w for SSA particles. Black solid and dashed lines denote ice saturation and expected homogeneous freezing, ¹³ respectively.

increase in the number of ice particles (Figure 5a, cyan line). This scan illustrates a case of homogeneous freezing, where no ice is formed until the SS_i reaches the homogeneous freezing threshold and nearly all the aerosol particles freeze. A similar trend was observed as RH was increased again beginning at 223 K, where in this particular case the SS_i reached even higher values (\sim 55%) before ice formation began. This observation is consistent with results from expansion chamber experiments using anhydrous NaCl particles starting at 235 K, wherein particles passed their DRH and subsequently froze via homogeneous freezing. In addition, the \sim 5% increase in RH_i

between 228 and 223 K follows closely with the expected homogeneous freezing conditions for fully dissolved particles.¹³

For CFDC scans of NaCl starting at colder temperatures (Figure 5b), ice nucleation behavior was considerably different. In the first scan starting at 218 K, ice formation was observed at a SS_i as low as 30%, with a gradual increase in the number of ice particles with increasing SS_i up to \sim 40% before the RH was reset to a lower value. Note the scans reset when the temperature (red line) dropped 5 K and produced a modest increase in supersaturations due to the T_{IW} decreasing faster

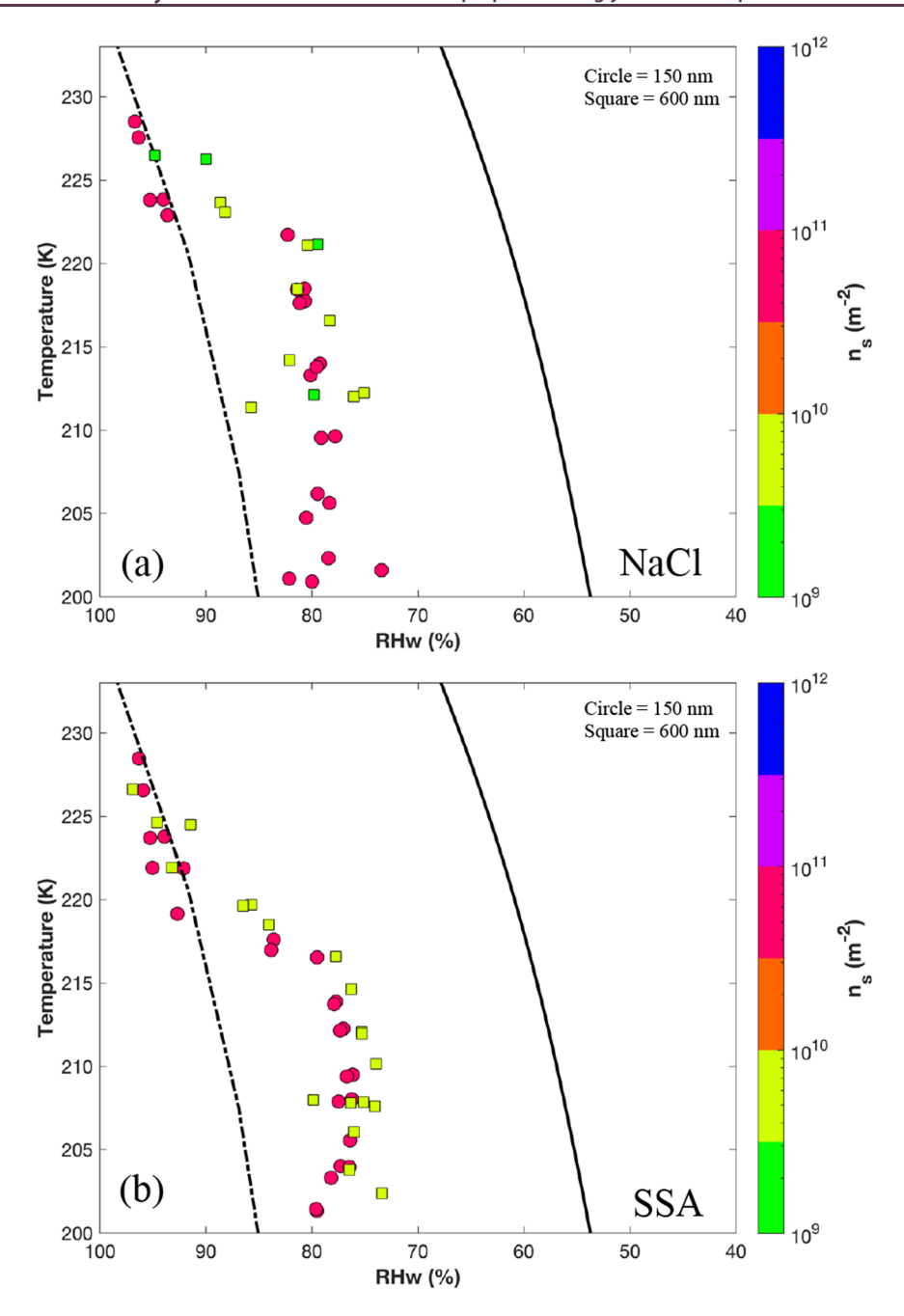


Figure 7. Ice active surface site density (n_s) magnitudes for a given RH_w and temperature for (a) NaCl and (b) SSAs at a 1% ice fraction. Circle and square markers indicate 150 and 600 nm particles, respectively. The black solid line indicates ice saturation, and the dashed line represents expected homogeneous freezing conditions.¹³

I

than the $T_{\rm OW}$. The second scan starting ~214 K showed a similar trend, and SS_i only reached 38% before the ice fraction reached 10% and the RH was brought back down. This SS_i was well below the highest SS_i that was reached during scans at warmer temperatures. These cases illustrate NaCl freezing through an apparent heterogeneous nucleation process since the onset of freezing occurred at ~30% SS_i, well below the threshold expected for homogeneous freezing. The ice nucleating behavior of SSA for 150 nm particles produced very similar trends as observed for NaCl (see the Supporting Information).

To elucidate the ice nucleating behaviors of differing aerosol sizes, Figure 6 shows the ice fractions of 1% and 10% freezing

in $T-\mathrm{RH_w}$ space for both sizes of NaCl and SSA particles at temperatures <230 K. The fraction freezing is based on ice concentrations divided by total CPC counts rather than OPC counts. Using the CPC provided a more reliable total aerosol count since the OPC may not have captured the smallest aerosols that were not deliquesced, particularly for the 150 nm experiments. Results using total aerosol counts from the OPC can be found in the Supporting Information. The color and shape of markers indicate the size and ice active fraction of the particles, where open markers denote 150 nm and filled denote 600 nm particles. Black solid and dashed lines denote ice saturation and the predicted homogeneous freezing threshold, 13 respectively. The majority of NaCl particles froze near

the homogeneous freezing line above 222 K. The 10% ice fraction observations above the homogeneous freezing line were within the range of uncertainties for the RH_w calculations (4%).⁷⁵ Below 222 K, there was a large decline in the required RH_w for 1% and 10% ice frozen fractions for both aerosol sizes shown in Figure 6a. For example, 1% freezing for both 150 and 600 nm NaCl particles occurred at ~80% RH_w, at 218 K, significantly lower than the 95% RH_w observed at 225 K. The onset of freezing for both sizes also occurred within proximity (~1%–3%) to the DRH line for anhydrous NaCl extrapolated to lower temperatures⁷⁰ (dashed cyan line). In general, our NaCl freezing results agreed well with results from previous lower temperature studies, all of which observed a shift from homogeneous freezing to heterogeneous nucleation as temperature decreased below 225 K.^{47,49,50}

Similar to NaCl, SSAs showed a transition from homogeneous freezing to heterogeneous nucleation (Figure 6b). However, the temperature at which this transition was observed, ~217 K, was nearly 5 K lower than that observed for NaCl, similar to observations made in a previous study comparing NaCl and SSA particles. ⁴⁷ The 5 K decrease in heterogeneous freezing onset for NaCl and SSA particles is likely a result of the lower DRH of SSAs.⁶¹ Because the eutectic point falls on the DRH line, this leads to a lower eutectic temperature for SSAs by about the same amount (~5 K) compared to pure NaCl particles. 66 Ice fractions of 1% and 10% below 215 K were observed 1%-3% RH_w lower than for NaCl particles at the same temperature. In general, SSA heterogeneous freezing at a 10% ice fraction aligned above the extrapolated DRH line, which was lowered by 4% RH_w for SSA, similar to the observed DRH in a previous study using synthetic seawater at low temperatures, 47 and 1% freezing conditions aligned near the DRH line, within RH_w uncertainty. This ice nucleating behavior of SSAs demonstrating freezing onsets at a slightly lower RH than NaCl has been shown in previous studies, 47,49 one of which used synthetic seawater and another that used a 1:1 synthetic sea salt and sucrose mixture. However, those studies differed on the inferred mode of heterogeneous freezing: the former attributed findings to possible deliquescence and immersion freezing since freezing occurred at the point where the liquid-solid transition was expected to initiate, and the latter inferred deposition freezing well below the DRH as the active mechanism. Particle sizes were different in those studies than used in this work, employing polydisperse distributions or supermicron particles.

Previous studies focusing on heterogeneous nucleation have used the ice nucleation active surface site density (n_s) as a parameter to determine the ice nucleation efficiency of aerosol particles for a given temperature and SS_i , normalized by the surface area. ^{7,47,76} Therefore, we calculated the n_s for SSAs and NaCl for both aerosol sizes, as shown in Figure 7. Average surface area concentrations per particle (S_a) for both aerosol sizes also accounted for DMA multiply charged particles using eq 2.

$$S_{a} = \sum_{i=1}^{6} (\pi N_{i} Dp_{i}^{2}) / \sum_{i=1}^{6} N_{i}$$
(2)

where N_i denotes the number concentration for each diameter with i positive charges, and Dp_i is the expected diameter with i positive charge. Values of n_{s} were then calculated by dividing the number of ice particles (N_{ice}) by the product of S_{a} and the total number of aerosols from the CPC (N_{a}) , as shown in eq 3.

$$n_{\rm s}(T, SS_{\rm i}) = \frac{N_{\rm ice}}{S_{\rm a}N_{\rm a}} \tag{3}$$

The inclusion of $N_{\rm a}$ serves as a scaling factor for $S_{\rm a}$ to the aerosol concentrations used in the experiments, since $S_{\rm a}$ was based on the generated size distributions, in which the aerosol concentrations were higher (Figure 3) due to the lack of dilution. In this manner, $S_{\rm a}$ still accounts for multiplet distributions and can be applied to the $N_{\rm ice}$ and $N_{\rm a}$ during experiments. While it is possible that the largest multiply charged particles freeze first due to thermodynamic considerations, that is both beyond the scope of the $n_{\rm s}$ framework and unsupported by our experimental data.

Figure 7 shows n_s magnitudes for SSA and NaCl, where circles represent 150 nm particles and squares represent 600 nm particles for 1% ice fraction. Magnitudes of n_s for 10% ice fraction can be found in the Supporting Information. In general, NaCl and SSA particles produced very similar (within a factor of 5) n_s magnitudes for each aerosol size, and the data suggested that higher n_s magnitudes were required for smaller particles to produce the same frozen fraction. The upper limit of 600 nm n_s magnitudes of $\sim 1 \times 10^{10}$ m⁻² also agreed well with previous n_s calculated values for 800 nm particles.⁴⁷ The most interesting feature of these results is the fact that ice onset was nearly the same regardless of the n_s values. Or, alternately, a strict association with the total particle surface area would have suggested that freezing onsets for the 600 nm particles would occur for the same n_s values as for 150 nm particles. This result implies that the n_s concept was not relevant for ice nucleation for SSAs in our study, either because features controlling freezing were not consistently distributed as a function of size or through a different mechanism. In other words, the process driving freezing of SSA particles at a low temperature occurred with the same efficiency regardless of the aerosol size or apparent geometric surface area.

4. DISCUSSION AND ATMOSPHERIC IMPLICATIONS

It is clear from this study that SSAs generated from natural seawater can initiate heterogeneous nucleation, and the similarities between NaCl and SSA particles for both aerosol sizes indicate that the freezing behavior may be dominated by the crystalline salts. The freezing behavior of NaCl and SSA particles as well as the n_s calculations from this study indicate that the size of lofted salt particles may not be an important factor for initiating heterogeneous nucleation. On the basis of our results, regardless of the surface area and site density, conditions supporting the onset of freezing for SSAs and NaCl particles remained largely the same. The higher n_s values for 150 nm particles at the same freezing onsets as 600 nm particles clearly violate the concept of active site density and suggest it is not applicable for NaCl and SSA particles. Instead, these results suggest little to no size dependence on the heterogeneous freezing behavior of SSAs and NaCl but rather dependence on the particle composition and thermodynamic conditions.

It remains difficult to determine what mode of freezing is controlling the onset of heterogeneous nucleation and the reason for the abrupt onset below a certain temperature threshold that differs between SSAs and NaCl particles. Deposition nucleation is an unlikely pathway for the SSA particles that freeze (in 1% frozen fraction) at below the DRH line since the initial water uptake of the additional salt components of SSAs would likely begin to occur at a RHw well

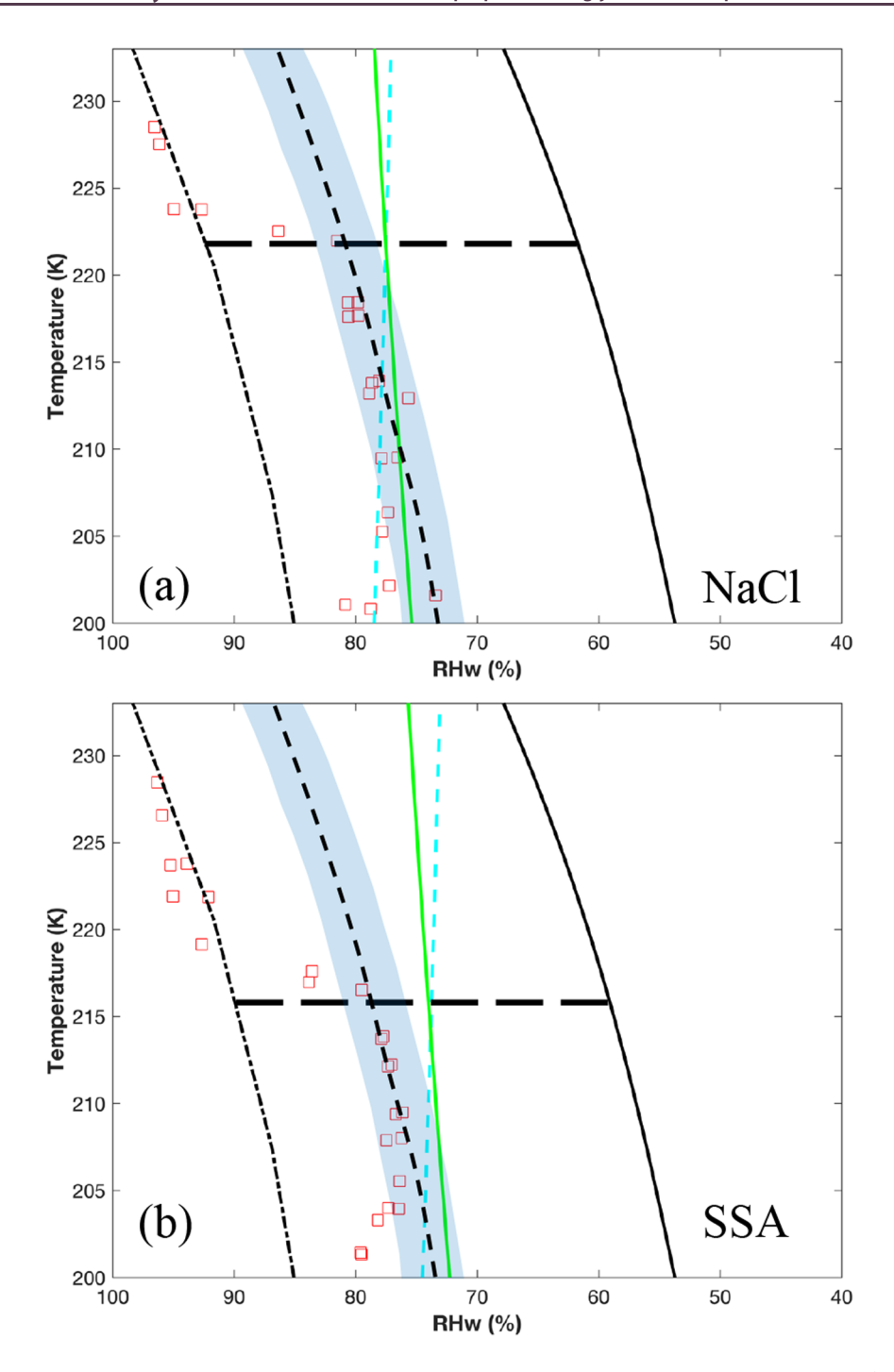


Figure 8. Conceptual diagram illustrating the competition between immersion freezing and pore-condensation freezing (PCF). Included are 1% frozen fraction for 150 nm particles denoted by the open squares. The solid green line indicates the parametrized RH_w for the onset of condensation into a 11.5 nm pore and 10 nm pore¹⁰ for NaCl and SSA particles, respectively. The dashed cyan line indicates the deliquescence relative humidity (DRH) for NaCl, extrapolated to cold temperatures and shifted toward a slightly lower RH_w for SSAs. The dashed black line indicates a constant Δa_{w} with uncertainties represented by the shaded blue region. The long dashed black line indicates the intersection of the PCF and DRH lines, indicative of the transition from homogeneous to heterogeneous nucleation.

below the DRH, 47,61 therefore discounting deposition as a nucleation mechanism. We consider two possible pathways for heterogeneous freezing for NaCl and SSA particles at cirrus conditions, as outlined in Figure 8. We simplify the discussion by including only 150 nm data at 1% frozen fraction. First, the immersion freezing mode, which is depicted as a required $\Delta a_{\rm w}$ with respect to the ice line, follows the previous application of the water activity concept of homogeneous freezing to the

heterogeneous freezing of mixtures of dissolved or partially dissolved particles. 15,16 It is possible to set a constant Δa_w , and thus nucleation rate, to align more or less with the data (short dashed line, with uncertainties indicated by the blue shading). For classical immersion freezing, the temperature threshold could be understood as the impact of the kinetic competition between full deliquescence and freezing, where, at higher temperatures, deliquescence would occur at progressively

lower $\mathrm{RH_w}$ values with respect to the onset $\mathrm{RH_w}$ for freezing, favoring full dissolution and homogeneous freezing. The long black dashed lines in Figure 8a,b indicate the transition point between homogeneous and heterogeneous freezing for NaCl and SSA particles, respectively, near the intersection of the lower bound of the immersion freezing envelope and the DRH line.

PCF is another potential mechanism that might be insensitive to particle size or surface area, explaining the existence of both the onset of heterogeneous freezing with decreasing temperature and the RHw onsets at a given temperature. In Figure 8, the solid green line represents the parametrized RH_w for the expected condensation of liquid water in a 11.5 and 10 nm pore 10 for NaCl and SSA particles, respectively, relevant to onset conditions of PCF, and the intersection of this condition with the DRH boundary becomes the controlling factor in governing the onset conditions of freezing. We note that the transition point between homogeneous and heterogeneous freezing does reasonably align with the intersection of the PCF (for the pore size chosen) and the DRH lines. If the PCF RH_w is above the DRH at a particular temperature, the pore freezing site is likely to be dissolved before it can activate heterogeneous freezing. If PCF RHw is below DRH, freezing may occur prior to dissolution. SSAs and NaCl particles produced from the drying of aqueous solutions are suspected to be highly porous, with observations of supermicron single particles, suggesting that SSAs are even more likely to form porous aggregates than NaCl. 68,77 In addition, dry submicron NaCl aerosols were found to retain more water at a low RH... than could be explained by solid crystalline NaCl morphologies.⁷⁷ That study states that their analysis is consistent with porous NaCl particles containing NaCl solution (rather than adsorbed water), although the exact morphology could not be identified. Another study examined water uptake in pores filled with soluble material, which may be similar to the water uptake behavior of pores formed in soluble material.⁷⁸ The freezing behavior of solution filled pores will depend on not only pore size but also solution concentration. 13,55 At sufficiently low temperatures, however, it seems reasonable to expect that if a sufficiently large pore activates and fills with solution it will subsequently freeze. In this regime, pore size is the controlling factor on the RHw where freezing occurs.

This PCF framework is a possible mechanism for the freezing of NaCl particles and may explain the transition temperature between homogeneous and heterogeneous freezing and the lack of differences between onset freezing conditions for the two sizes. However, PCF would require the particles to be fully dry, which is unlikely for SSAs at these temperatures. The additional calcium and magnesium salts in SSAs, which have lower deliquescence points, 61 as well as the presence of organics, would allow for partial deliquescence at a lower RH_w than for the NaCl core. In addition, previous studies have shown that, even after efflorescence, SSA particles may retain up to 5–10 wt % of residual water. 61,67,79 The more likely scenario is the development of a brine layer for SSAs as the RH_w approaches the DRH, which has been observed in two previous studies using inorganic SSA particles. 47,49 Schill and Tolbert in 2014 were able to visually observe a brine layer encompassing an inorganic sea salt particle at 59% RHw, and using laser light scattering intensity and a linear depolarization ratio, Wagner et al. in 2018 also concluded the presence of a brine layer on SSAs. Therefore, PCF is not a viable freezing

mechanism under these circumstances because the surface pores would dissolve and inhibit freezing via this pathway. Instead, both previous studies concluded the formation of a brine layer helped to initiate immersion freezing. However, one difference was that Schill and Tolbert in 2014 observed much lower freezing onsets ~68% RH_w for their 1:1 ratio sucrose to synthetic sea-salt particles compared to SSA particles in Wagner et al. in 2018. This may indicate that the dissolution of the particles is dictated by the organics present, and it is unclear whether a sucrose mixture is representative of the organic components of SSAs. The onset freezing results from this study are most consistent with the previous work of Wagner et al. in 2018 on the heterogeneous freezing of SSA, confirming immersion freezing as the likely pathway for SSA below 220 K. The lack of size effects must be explained by the concentration of solution on the particle surface controlling the immersion freezing but would require a further inspection of the rates of dissolution and dilution in different size classes and probing of their relative compositions. This result may also explain why the surface area normalization does not work for SSA because the dry surface area is not relevant for a partially dissolved salt crystal acting as the freezing site. It is presently unclear the reason for the similar heterogeneous freezing behavior between NaCl and SSA particles and seemingly very different freezing mechanisms, which will warrant future study.

In this study, we found that particles produced from natural SW spray froze via heterogeneous nucleation at conditions similar to those reported in previous studies. 47,49 We have demonstrated the ability to replicate and augment the heterogeneous freezing results of NaCl particles and SSAs from the AIDA cloud chamber⁴⁷ in easily conducted scans using a CFDC. An advantage to this instrument and the scanning procedure employed is that the nature of the CFDC allows for the study of particle response over a full profile of RH_w up to water saturation for any temperature (i.e., the limitations imposed by ice formation depleting water vapor in an expansion cloud chamber do not exist), which allows for studies relevant to cirrus cloud ice nucleation over a wide range of environmental conditions. The method could be extended to measurements on ambient particles, for which there exists a dearth of data for freezing behaviors at these temperatures and humidities.

Our results illustrate the potential of SSAs to be a significant source of INPs in the cirrus regime. For both aerosol sizes, up to 10% of the SSA population froze below 80% $RH_{\rm w}$ at temperatures <225 K. SSA concentrations in the upper troposphere range from 10^{-4} to $10^{-1} \mu g m^{-3}$, and assuming a density of 2.2 g cm⁻³,⁷² the upper and lower bounds of 150 and 600 nm particles could be in the range $10^{-1}-10^4$ L⁻¹. Since average ice crystal number concentrations in cirrus clouds range between 0.01 and 10 L⁻¹ depending on latitudinal location, 21,22,80 the projected population of SSA-derived INPs would represent a significant source of heterogeneous INPs for cirrus clouds. In the absence of significant numbers of other efficient INPs, such as mineral dusts, one could expect SSAs to be strongly competing or dominating ice formation. In addition, size distributions of SSA above 4 km were found to be dominated by sizes <400 nm. ³⁶ Therefore, the aerosol sizes chosen in this study may be more representative of the sizes of SSA active in the cirrus regime as opposed to previous studies that used aerosols 800 nm or larger. 47,49,51 These results represent a strong case for explaining the observations of SSAs as a cirrus INP in previous studies of cirrus IR over the tropical

and subtropical oceans.²⁵ Although that study concluded that the dominant sources of cirrus INPs were mineral dust and metallic particles, the flights that took place over the ocean were located predominantly downstream of major sources of dust and pollution, and SSAs still made up substantial fractions of IR when in direct competition with efficient INPs like mineral dust. It is unclear what fraction of IR would be sea salts if flights occurred over more pristine ocean regions, and this may warrant future exploration.

When discussing SSAs as a source of heterogeneous INPs, it is important to address the origin of the cirrus, liquid versus in situ origin, as this could determine by which nucleation mechanism SSAs would initiate freezing (i.e., homogeneous versus heterogeneous freezing). SSAs in liquid origin cirrus would likely remain as aqueous solutions and initiate homogeneous freezing. However, SSAs may be present at cirrus levels in effloresced crystalline structures and initiate heterogeneous nucleation to form in situ origin cirrus. There are a number of different scenarios where the latter case may occur. First, SSAs are lofted to cirrus temperatures via deep convective updrafts and detrained in anvils, specifically in the tropics where cirrus clouds are most frequently observed.⁸¹ However, it would require the SSA particles to encounter dry air and effloresce; understanding how often this particular scenario occurs is beyond the scope of this study. Second, warm conveyor belts associated with lofting of air in frontal systems are known to be the most frequent source of in situ cirrus, 22,23 which may occur over some ocean regions and bring SSAs to high altitudes and lower temperatures. An example of this scenario may be large storm tracks over the Northern Atlantic where in situ origin cirrus can be present ~70% and >50% of the time above 200 hPa or below 220 K,82,83 respectively.

We have shown that SSAs have the potential to initiate heterogeneous nucleation at temperatures below 220 K. It is known that cirrus clouds have the potential to warm or cool the atmosphere depending on their formation mechanism and origin type. The heterogeneous nucleation of SSAs would drive the formation of the in situ origin type cirrus, which are shown to produce a net positive radiative forcing. This illustrates a potentially significant indirect effect of SSAs in the cirrus regime. Since SSA concentrations are strongly modulated by sea-surface temperatures, as well as surface winds, changes in SSA generation and lofting to the upper troposphere may represent an important aerosol-cloud interaction that should be studied in assessing atmospheric response in a warming future climate.

ASSOCIATED CONTENT

Supporting Information

The Supporting Information is available free of charge at https://pubs.acs.org/doi/10.1021/acsearthspace-chem.1c00228.

Discussions of flow calculation, annular forced flow, annular convective flow, volume to mass flow conversion, annular water vapor profiles, and comparisons to previous calculations and figures of comparison between previous and current flow calculations, CFDC time series for SSA experiments, ice fractions for NaCl-and SSA-generated particles, and ice active surface site density magnitudes (PDF)

AUTHOR INFORMATION

Corresponding Author

Ryan J. Patnaude — Department of Atmospheric Sciences, Colorado State University, Fort Collins, Colorado 80523, United States; orcid.org/0000-0003-3129-8279; Email: ryan.patnaude@colostate.edu

Authors

- Russell J. Perkins Department of Atmospheric Sciences, Colorado State University, Fort Collins, Colorado 80523, United States
- Sonia M. Kreidenweis Department of Atmospheric Sciences, Colorado State University, Fort Collins, Colorado 80523, United States
- Paul J. DeMott Department of Atmospheric Sciences, Colorado State University, Fort Collins, Colorado 80523, United States

Complete contact information is available at: https://pubs.acs.org/10.1021/acsearthspacechem.1c00228

Author Contributions

The manuscript was written through contributions of all authors. All authors have given approval to the final version of the manuscript.

Notes

The authors declare no competing financial interest.

ACKNOWLEDGMENTS

This work was supported by the National Science Foundation (NSF) through the NSF Center for Aerosol Impacts on Chemistry of the Environment (NSF-CAICE), Award CHE-1801971. The authors would also like to acknowledge the reviewers of this manuscript for their helpful comments and suggestions.

■ REFERENCES

- (1) Baker, M. B. Cloud Microphysics and Climate. Science (Washington, DC, U. S.) 1997, 276 (5315), 1072-1078.
- (2) Liou, K.-N. Influence of Cirrus Clouds on Weather and Climate Processes: A Global Perspective. *Mon. Weather Rev.* **1986**, *114* (6), 1167–1199.
- (3) Lynch, D. K. Cirrus Clouds: Their Role in Climate and Global Change. *Acta Astronaut.* **1996**, 38 (11), 859–863.
- (4) Zhang, Y.; MacKe, A.; Albers, F. Effect of Crystal Size Spectrum and Crystal Shape on Stratiform Cirrus Radiative Forcing. *Atmos. Res.* **1999**, *52* (1), 59–75.
- (5) Jensen, E. J.; Kinne, S.; Toon, O. B. Tropical Cirrus Cloud Radiative Forcing: Sensitivity Studies. *Geophys. Res. Lett.* **1994**, *21* (18), 2023–2026.
- (6) Heymsfield, A. J.; Krämer, M.; Luebke, A.; Brown, P.; Cziczo, D. J.; Franklin, C.; Lawson, P.; Lohmann, U.; McFarquhar, G.; Ulanowski, Z.; Van Tricht, K. Cirrus Clouds. *Meteorol. Monogr.* 2017, 58, 2.1–2.26.
- (7) Hoose, C.; Möhler, O. Heterogeneous Ice Nucleation on Atmospheric Aerosols: A Review of Results from Laboratory Experiments. *Atmos. Chem. Phys.* **2012**, *12* (20), 9817.
- (8) Vali, G.; DeMott, P. J.; Möhler, O.; Whale, T. F. Technical Note: A Proposal for Ice Nucleation Terminology. *Atmos. Chem. Phys.* **2015**, 15 (18), 10263–10270.
- (9) Kanji, Z. A.; Ladino, L. A.; Wex, H.; Boose, Y.; Burkert-Kohn, M.; Cziczo, D. J.; Krämer, M. Overview of Ice Nucleating Particles. *Meteorol. Monogr.* **2017**, *58* (1), 1.1–1.33.
- (10) Marcolli, C. Deposition Nucleation Viewed as Homogeneous or Immersion Freezing in Pores and Cavities. *Atmos. Chem. Phys.* **2014**, *14* (4), 2071–2104.

- (11) Campbell, J. M.; Meldrum, F. C.; Christenson, H. K. Observing the Formation of Ice and Organic Crystals in Active Sites. *Proc. Natl. Acad. Sci. U. S. A.* **2017**, *114* (5), 810–815.
- (12) David, R. O.; Marcolli, C.; Fahrni, J.; Qiu, Y.; Perez Sirkin, Y. A.; Molinero, V.; Mahrt, F.; Brühwiler, D.; Lohmann, U.; Kanji, Z. A. Pore Condensation and Freezing Is Responsible for Ice Formation below Water Saturation for Porous Particles. *Proc. Natl. Acad. Sci. U. S. A.* **2019**, *116* (17), 8184–8189.
- (13) Koop, T.; Luo, B.; Tsias, A.; Peter, T. Water Activity as the Determinant for Homogeneous Ice Nucleation in Aqueous Solutions. *Nature* **2000**, *406*, 611–614.
- (14) DeMott, P. J.; Cziczo, D. J.; Prenni, A. J.; Murphy, D. M.; Kreidenweis, S. M.; Thomson, D. S.; Borys, R.; Rogers, D. C. Measurements of the Concentration and Composition of Nuclei for Cirrus Formation. *Proc. Natl. Acad. Sci. U. S. A.* **2003**, *100* (25), 14655–14660.
- (15) Zuberi, B.; Bertram, A. K.; Cassa, C. A.; Molina, L. T.; Molina, M. J. Heterogeneous Nucleation of Ice in (NH₄)₂SO₄-H₂O Particles with Mineral Dust Immersions. *Geophys. Res. Lett.* **2002**, 29 (10), 142-1
- (16) Archuleta, C. M.; DeMott, P. J.; Kreidenweis, S. M. Ice Nucleation by Surrogates for Atmospheric Mineral Dust and Mineral Dust/Sulfate Particles at Cirrus Temperatures. *Atmos. Chem. Phys.* **2005**, *5* (10), 2617–2634.
- (17) DeMott, P. J.; Rogers, D. C.; Kreidenweis, S. M. The Susceptibility of Ice Formation in Upper Tropospheric Clouds to Insoluble Aerosol Components. *J. Geophys. Res. Atmos.* **1997**, *102* (D16), 19575–19584.
- (18) Kärcher, B.; Lohmann, U. A Parameterization of Cirrus Cloud Formation: Heterogeneous Freezing. *J. Geophys. Res.* **2003**, *108* (D14), 4402.
- (19) Haag, W.; Kärcher, B.; Ström, J.; Minikin, A.; Lohmann, U.; Ovarlez, J.; Stohl, A. Freezing Thresholds and Cirrus Cloud Formation Mechanisms Inferred from in Situ Measurements of Relative Humidity. *Atmos. Chem. Phys.* **2003**, *3* (5), 1791–1806.
- (20) Gierens, K. On the Transition between Heterogeneous and Homogeneous Freezing. *Atmos. Chem. Phys.* **2003**, 3 (2), 437–446.
- (21) Krämer, M.; Schiller, C.; Afchine, A.; Bauer, R.; Gensch, I.; Mangold, A.; Schlicht, S.; Spelten, N.; Sitnikov, N.; Borrmann, S.; De Reus, M.; Spichtinger, P. Ice Supersaturations and Cirrus Cloud Crystal Numbers. *Atmos. Chem. Phys.* **2009**, *9* (11), 3505–3522.
- (22) Krämer, M.; Rolf, C.; Spelten, N.; Afchine, A.; Fahey, D.; Jensen, E.; Khaykin, S.; Kuhn, T.; Lawson, P.; Lykov, A.; L. Pan, L.; Riese, M.; Rollins, A.; Stroh, F.; Thornberry, T.; Wolf, V.; Woods, S.; Spichtinger, P.; Quaas, J.; Sourdeval, O. A Microphysics Guide to Cirrus Part 2: Climatologies of Clouds and Humidity from Observations. *Atmos. Chem. Phys.* **2020**, 20 (21), 12569–12608.
- (23) Krämer, M.; Rolf, C.; Luebke, A.; Afchine, A.; Spelten, N.; Costa, A.; Meyer, J.; Zöger, M.; Smith, J.; Herman, R. L.; Buchholz, B.; Ebert, V.; Baumgardner, D.; Borrmann, S.; Klingebiel, M.; Avallone, L. A Microphysics Guide to Cirrus Clouds Part 1: Cirrus Types. Atmos. Chem. Phys. 2016, 16 (5), 3463—3483.
- (24) Luebke, A. E.; Afchine, A.; Costa, A.; Grooß, J. U.; Meyer, J.; Rolf, C.; Spelten, N.; M Avallone, L.; Baumgardner, D.; Krämer, M. The Origin of Midlatitude Ice Clouds and the Resulting Influence on Their Microphysical Properties. *Atmos. Chem. Phys.* **2016**, *16* (9), 5793–5809.
- (25) Cziczo, D. J.; Froyd, K. D.; Hoose, C.; Jensen, E. J.; Diao, M.; Zondlo, M. A.; Smith, J. B.; Twohy, C. H.; Murphy, D. M. Clarifying the Dominant Sources and Mechanisms of Cirrus Cloud Formation. *Science (Washington, DC, U. S.)* **2013**, 340 (6138), 1320–1324.
- (26) Boucher, O.; Randall, D.; Artaxo, P.; Bretherton, C.; Feingold, G.; Forster, P.; Kerminen, V.-M.; Kondo, Y.; Liao, H.; Lohmann, U.; Rasch, P.; Satheesh, S. K.; Sherwood, S. C.; Stevens, B.; Zhang, X.-Y. Clouds and Aerosols. Climate Change 2013 the Physical Science Basis: Working Group I Contribution to the Fifth Assessment Report of the Intergovernmental Panel on Climate Change; Cambridge University Press, 2013; pp 571–658.

- (27) Cziczo, D. J.; Froyd, K. D. Sampling the Composition of Cirrus Ice Residuals. *Atmos. Res.* **2014**, *142*, 15–31.
- (28) Cziczo, D. J.; Murphy, D. M.; Hudson, P. K.; Thomson, D. S. Single Particle Measurements of the Chemical Composition of Cirrus Ice Residue during CRYSTAL-FACE. *J. Geophys. Res. Atmos.* **2004**, *109*, D04201.
- (29) Froyd, K. D.; Murphy, S. M.; Murphy, D. M.; De Gouw, J. A.; Eddingsaas, N. C.; Wennberg, P. O. Contribution of Isoprene-Derived Organosulfates to Free Tropospheric Aerosol Mass. *Proc. Natl. Acad. Sci. U. S. A.* **2010**, *107* (50), 21360–21365.
- (30) Schill, G. P.; Froyd, K. D.; Bian, H.; Kupc, A.; Williamson, C.; Brock, C. A.; Ray, E.; Hornbrook, R. S.; Hills, A. J.; Apel, E. C.; Chin, M.; Colarco, P. R.; Murphy, D. M. Widespread Biomass Burning Smoke throughout the Remote Troposphere. *Nat. Geosci.* **2020**, *13* (6), 422–427.
- (31) Schwarz, J. P.; Weinzierl, B.; Samset, B. H.; Dollner, M.; Heimerl, K.; Markovic, M. Z.; Perring, A. E.; Ziemba, L. Aircraft Measurements of Black Carbon Vertical Profiles Show Upper Tropospheric Variability and Stability. *Geophys. Res. Lett.* **2017**, 44 (2), 1132–1140.
- (32) Mahrt, F.; Kilchhofer, K.; Marcolli, C.; Grönquist, P.; David, R. O.; Rösch, M.; Lohmann, U.; Kanji, Z. A. The Impact of Cloud Processing on the Ice Nucleation Abilities of Soot Particles at Cirrus Temperatures. *J. Geophys. Res.: Atmos.* **2020**, *125* (3), 1–23.
- (33) Wolf, M. J.; Zhang, Y.; Zawadowicz, M. A.; Goodell, M.; Froyd, K.; Freney, E.; Sellegri, K.; Rösch, M.; Cui, T.; Winter, M.; Lacher, L.; Axisa, D.; DeMott, P. J.; Levin, E. J. T.; Gute, E.; Abbatt, J.; Koss, A.; Kroll, J. H.; Surratt, J. D.; Cziczo, D. J. A Biogenic Secondary Organic Aerosol Source of Cirrus Ice Nucleating Particles. *Nat. Commun.* 2020, 11 (4834), 4834.
- (34) O'Dowd, C. D.; Smith, M. H.; Consterdine, I. E.; Lowe, J. A. Marine Aerosol, Sea-Salt, and the Marine Sulphur Cycle: A Short Review. *Atmos. Environ.* **1997**, *31* (1), 73–80.
- (35) Twohy, C. H.; Poellot, M. R. Chemical Characteristics of Ice Residual Nuclei in Anvil Cirrus Clouds: Evidence for Homogeneous and Heterogeneous Ice Formation. *Atmos. Chem. Phys.* **2005**, *5* (8), 2289–2297.
- (36) Murphy, D. M.; Froyd, K. D.; Bian, H.; Brock, C. A.; Dibb, J. E.; Digangi, J. P.; Diskin, G.; Dollner, M.; Kupc, A.; Scheuer, E. M.; Schill, G. P.; Weinzierl, B.; Williamson, C. J.; Yu, P. The Distribution of Sea-Salt Aerosol in the Global Troposphere. *Atmos. Chem. Phys.* **2019**, *19* (6), 4093–4104.
- (37) Bian, H.; Froyd, K.; Murphy, D. M.; Dibb, J.; Darmenov, A.; Chin, M.; Colarco, P. R.; Da Silva, A.; Kucsera, T. L.; Schill, G.; Yu, H.; Bui, P.; Dollner, M.; Weinzierl, B.; Smirnov, A. Observationally Constrained Analysis of Sea Salt Aerosol in the Marine Atmosphere. *Atmos. Chem. Phys.* **2019**, *19* (16), 10773–10785.
- (38) Murphy, D. M.; Thomson, D. S.; Mahoney, M. J. In Situ Measurements of Organics, Meteoritic Material, Mercury, and Other Elements in Aerosols at 5 to 19 Kilometers. *Science* (80-.). **1998**, 282 (5394), 1664–1669.
- (39) Chen, Y.; Kreidenweis, S. M.; McInnes, L. M.; Rogers, D. C.; DeMott, P. J. Single Particle Analyses of Ice Nucleating Aerosols in the Upper Troposphere and Lower Stratosphere. *Geophys. Res. Lett.* **1998**, 25 (9), 1391–1394.
- (40) Abbatt, J. P. D.; Benz, S.; Cziczo, D. J.; Kanji, Z.; Lohmann, U.; Möhler, O. Solid Ammonium Sulfate Aerosols as Ice Nuclei: A Pathway for Cirrus Cloud Formation. *Science (Washington, DC, U. S.)* **2006**, *313* (5794), 1770–1773.
- (41) Sassen, K.; Arnott, W. P.; Starr, D. O. C.; Mace, G. G.; Wang, Z.; Poellot, M. R. Midlatitude Cirrus Clouds Derived from Hurricane Nora: A Case Study with Implications for Ice Crystal Nucleation and Shape. *J. Atmos. Sci.* **2003**, *60* (7), 873–891.
- (42) Wilson, T. W.; Ladino, L. A.; Alpert, P. A.; Breckels, M. N.; Brooks, I. M.; Browse, J.; Burrows, S. M.; Carslaw, K. S.; Huffman, J. A.; Judd, C.; Kilthau, W. P.; Mason, R. H.; McFiggans, G.; Miller, L. A.; Najera, J. J.; Polishchuk, E.; Rae, S.; Schiller, C. L.; Si, M.; Temprado, J. V.; Whale, T. F.; Wong, J. P. S.; Wurl, O.; Yakobi-Hancock, J. D.; Abbatt, J. P. D.; Aller, J. Y.; Bertram, A. K.; Knopf, D.

- A.; Murray, B. J. A Marine Biogenic Source of Atmospheric Ice-Nucleating Particles. *Nature* **2015**, 525, 234–238.
- (43) O'Dowd, C. D.; De Leeuw, G. Marine Aerosol Production: A Review of the Current Knowledge. *Philos. Trans. R. Soc., A* **2007**, 365 (1856), 1753–1774.
- (44) Gantt, B.; Meskhidze, N. The Physical and Chemical Characteristics of Marine Primary Organic Aerosol: A Review. *Atmos. Chem. Phys.* **2013**, *13* (8), 3979–3996.
- (45) Prather, K. A.; Bertram, T. H.; Grassian, V. H.; Deane, G. B.; Stokes, M. D.; DeMott, P. J.; Aluwihare, L. I.; Palenik, B. P.; Azam, F.; Seinfeld, J. H.; Moffet, R. C.; Molina, M. J.; Cappa, C. D.; Geiger, F. M.; Roberts, G. C.; Russell, L. M.; Ault, A. P.; Baltrusaitis, J.; Collins, D. B.; Corrigan, C. E.; Cuadra-Rodriguez, L. A.; Ebben, C. J.; Forestieri, S. D.; Guasco, T. L.; Hersey, S. P.; Kim, M. J.; Lambert, W. F.; Modini, R. L.; Mui, W.; Pedler, B. E.; Ruppel, M. J.; Ryder, O. S.; Schoepp, N. G.; Sullivan, R. C.; Zhao, D. Bringing the Ocean into the Laboratory to Probe the Chemical Complexity of Sea Spray Aerosol. *Proc. Natl. Acad. Sci. U. S. A.* 2013, 110 (19), 7550–7555.
- (46) Mccluskey, C. S.; Hill, E. T. C. J.; Sultana, C. M.; Laskina, O.; Trueblood, J.; Santander, M. V.; Beall, C. M.; Michaud, J. M.; Kreidenweis, S. M.; Prather, K. A.; Grassian, V.; Demott, P. J. A Mesocosm Double Feature: Insights into the Chemical Makeup of Marine Ice Nucleating Particles. *J. Atmos. Sci.* **2018**, 75 (7), 2405–2423.
- (47) Wagner, R.; Kaufmann, J.; Möhler, O.; Saathoff, H.; Schnaiter, M.; Ullrich, R.; Leisner, T. Heterogeneous Ice Nucleation Ability of NaCl and Sea Salt Aerosol Particles at Cirrus Temperatures. *J. Geophys. Res.: Atmos.* **2018**, 123 (5), 2841–2860.
- (48) Wolf, M. J.; Coe, A.; Dove, L. A.; Zawadowicz, M. A.; Dooley, K.; Biller, S. J.; Zhang, Y.; Chisholm, S. W.; Cziczo, D. J. Investigating the Heterogeneous Ice Nucleation of Sea Spray Aerosols Using Prochlorococcus as a Model Source of Marine Organic Matter. *Environ. Sci. Technol.* **2019**, *53* (3), 1139–1149.
- (49) Schill, G. P.; Tolbert, M. A. Heterogeneous Ice Nucleation on Simulated Sea-Spray Aerosol Using Raman Microscopy. *J. Phys. Chem.* C **2014**, *118* (50), 29234–29241.
- (50) Ladino, L. A.; Yakobi-Hancock, J. D.; Kilthau, W. P.; Mason, R. H.; Si, M.; Li, J.; Miller, L. A.; Schiller, C. L.; Huffman, J. A.; Aller, J. Y.; Knopf, D. A.; Bertram, A. K.; Abbatt, J. P. D. Addressing the Ice Nucleating Abilities of Marine Aerosol: A Combination of Deposition Mode Laboratory and Field Measurements. *Atmos. Environ.* **2016**, 132, 1–10.
- (51) Wagner, R.; Ickes, L.; Bertram, A. K.; Els, N.; Gorokhova, E.; Möhler, O.; Murray, B. J.; Umo, N. S.; Salter, M. E. Heterogeneous Ice Nucleation Ability of Aerosol Particles Generated from Arctic Sea Surface Microlayer and Surface Seawater Samples at Cirrus Temperatures. Atmos. Chem. Phys. Discuss., in press, 2021.
- (52) Knopf, D. A.; Alpert, P. A.; Wang, B. The Role of Organic Aerosol in Atmospheric Ice Nucleation: A Review. ACS Earth Sp. Chem. 2018, 2 (3), 168–202.
- (53) Zhang, Y.; Nichman, L.; Spencer, P.; Jung, J. I.; Lee, A.; Heffernan, B. K.; Gold, A.; Zhang, Z.; Chen, Y.; Canagaratna, M. R.; Jayne, J. T.; Worsnop, D. R.; Onasch, T. B.; Surratt, J. D.; Chandler, D.; Davidovits, P.; Kolb, C. E. The Cooling Rate- And Volatility-Dependent Glass-Forming Properties of Organic Aerosols Measured by Broadband Dielectric Spectroscopy. *Environ. Sci. Technol.* **2019**, 53 (21), 12366–12378.
- (54) Ignatius, K.; Kristensen, T. B.; Järvinen, E.; Nichman, L.; Fuchs, C.; Gordon, H.; Herenz, P.; Hoyle, C. R.; Duplissy, J.; Garimella, S.; Dias, A.; Frege, C.; Höppel, N.; Tröstl, J.; Wagner, R.; Yan, C.; Amorim, A.; Baltensperger, U.; Curtius, J.; Donahue, N. M.; Gallagher, M. W.; Kirkby, J.; Kulmala, M.; Möhler, O.; Saathoff, H.; Schnaiter, M.; Tomé, A.; Virtanen, A.; Worsnop, D.; Stratmann, F. Heterogeneous Ice Nucleation of Viscous Secondary Organic Aerosol Produced from Ozonolysis of α -Pinene. *Atmos. Chem. Phys.* **2016**, *16* (10), 6495–6509.
- (55) Zobrist, B.; Marcolli, C.; Pedernera, D. A.; Koop, T. Do Atmospheric Aerosols Form Glasses? *Atmos. Chem. Phys.* **2008**, 8 (17), 5221–5244.

- (56) Murray, B. J.; Wilson, T. W.; Dobbie, S.; Cui, Z.; Al-Jumur, S. M. R. K.; Möhler, O.; Schnaiter, M.; Wagner, R.; Benz, S.; Niemand, M.; Saathoff, H.; Ebert, V.; Wagner, S.; Kärcher, B. Heterogeneous Nucleation of Ice Particles on Glassy Aerosols under Cirrus Conditions. *Nat. Geosci.* **2010**, *3*, 233–237.
- (57) Berkemeier, T.; Shiraiwa, M.; Pöschl, U.; Koop, T. Competition between Water Uptake and Ice Nucleation by Glassy Organic Aerosol Particles. *Atmos. Chem. Phys.* **2014**, *14* (22), 12513–12531.
- (58) Wagner, R.; Möhler, O. Heterogeneous Ice Nucleation Ability of Crystalline Sodium Chloride Dihydrate Particles. *J. Geophys. Res. Atmos.* **2013**, *118* (10), 4610–4622.
- (59) Wise, M. E.; Baustian, K. J.; Koop, T.; Freedman, M. A.; Jensen, E. J.; Tolbert, M. A. Depositional Ice Nucleation onto Crystalline Hydrated NaCl Particles: A New Mechanism for Ice Formation in the Troposphere. *Atmos. Chem. Phys.* **2012**, *12* (2), 1121–1134.
- (60) Kong, X.; Wolf, M. J.; Roesch, M.; Thomson, E. S.; Bartels-Rausch, T.; Alpert, P. A.; Ammann, M.; Prisle, N. L.; Cziczo, D. J. A Continuous Flow Diffusion Chamber Study of Sea Salt Particles Acting as Cloud Nuclei: Deliquescence and Ice Nucleation. *Tellus, Ser. B* **2018**, *70* (1), 1–11.
- (61) Tang, I. N.; Tridico, A. C.; Fung, K. H. Thermodynamic and Optical Properties of Sea Salt Aerosols. *J. Geophys. Res. Atmos.* **1997**, 102 (D19), 23269–23275.
- (62) Rogers, D. C. Development of a Continuous Flow Thermal Gradient Diffusion Chamber for Ice Nucleation Studies. *Atmos. Res.* **1988**, 22 (2), 149–181.
- (63) DeMott, P. J.; Petters, M. D.; Prenni, A. J.; Carrico, C. M.; Kreidenweis, S. M.; Collett, J. L.; Moosmüller, H. Ice Nucleation Behavior of Biomass Combustion Particles at Cirrus Temperatures. *J. Geophys. Res.* **2009**, *114* (D16), D16205.
- (64) Rogers, D. C.; DeMott, P. J.; Kreidenweis, S. M.; Chen, Y. A Continuous-Flow Diffusion Chamber for Airborne Measurements of Ice Nuclei. *J. Atmos. Ocean. Technol.* **2001**, *18* (5), 725–741.
- (65) DeMott, P. J.; Prenni, A. J.; McMeeking, G. R.; Sullivan, R. C.; Petters, M. D.; Tobo, Y.; Niemand, M.; Möhler, O.; Snider, J. R.; Wang, Z.; Kreidenweis, S. M. Integrating Laboratory and Field Data to Quantify the Immersion Freezing Ice Nucleation Activity of Mineral Dust Particles. *Atmos. Chem. Phys.* **2015**, *15* (1), 393–409.
- (66) Martin, S. T. Phase Transitions of Aqueous Atmospheric Particles. *Chem. Rev.* **2000**, *100* (9), 3403–3453.
- (67) Koop, T.; Kapilashrami, A.; Molina, L. T.; Molina, M. J. Phase Transitions of Sea-Salt/Water Mixtures at Low Temperatures: Implications for Ozone Chemistry in the Polar Marine Boundary Layer. J. Geophys. Res. Atmos. 2000, 105 (D21), 26393–26402.
- (68) Peckhaus, A.; Kiselev, A.; Wagner, R.; Duft, D.; Leisner, T. Temperature-Dependent Formation of NaCl Dihydrate in Levitated NaCl and Sea Salt Aerosol Particles. *J. Chem. Phys.* **2016**, *145* (24), 244503.
- (69) Bertram, T. H.; Cochran, R. E.; Grassian, V. H.; Stone, E. A. Sea Spray Aerosol Chemical Composition: Elemental and Molecular Mimics for Laboratory Studies of Heterogeneous and Multiphase Reactions. *Chem. Soc. Rev.* **2018**, *47* (7), 2374–2400.
- (70) Tang, I. N.; Munkelwitz, H. R. Composition and Temperature Dependence of the Deliquescence Properties of Hygroscopic Aerosols. *Atmos. Environ., Part A* **1993**, *27* (4), 467–473.
- (71) Zieger, P.; Väisänen, O.; Corbin, J. C.; Partridge, D. G.; Bastelberger, S.; Mousavi-Fard, M.; Rosati, B.; Gysel, M.; Krieger, U. K.; Leck, C.; Nenes, A.; Riipinen, I.; Virtanen, A.; Salter, M. E. Revising the Hygroscopicity of Inorganic Sea Salt Particles. *Nat. Commun.* **2017**, *8*, 15883.
- (72) Brock, C. A.; Williamson, C.; Kupc, A.; Froyd, K. D.; Erdesz, F.; Wagner, N.; Richardson, M.; Schwarz, J. P.; Gao, R. S.; Katich, J. M.; Campuzano-Jost, P.; Nault, B. A.; Schroder, J. C.; Jimenez, J. L.; Weinzierl, B.; Dollner, M.; Bui, T.; Murphy, D. M. Aerosol Size Distributions during the Atmospheric Tomography Mission (ATom): Methods, Uncertainties, and Data Products. *Atmos. Meas. Tech.* **2019**, *12* (6), 3081–3099.

- (73) Quinn, P. K.; Collins, D. B.; Grassian, V. H.; Prather, K. A.; Bates, T. S. Chemistry and Related Properties of Freshly Emitted Sea Spray Aerosol. *Chem. Rev.* **2015**, *115* (10), 4383–4399.
- (74) Collins, D. B.; Zhao, D. F.; Ruppel, M. J.; Laskina, O.; Grandquist, J. R.; Modini, R. L.; Stokes, M. D.; Russell, L. M.; Bertram, T. H.; Grassian, V. H.; Deane, G. B.; Prather, K. A. Direct Aerosol Chemical Composition Measurements to Evaluate the Physicochemical Differences between Controlled Sea Spray Aerosol Generation Schemes. *Atmos. Meas. Tech.* **2014**, *7* (11), 3667–3683.
- (75) Richardson, M. Making Real Time Measurements of Ice Nuclei Concentrations at Upper Tropospheric Temperatures: Extending the Capabilities of the Continuous Flow Diffusion; Colorado State University, 2009.
- (76) Connolly, P. J.; Möhler, O.; Field, P. R.; Saathoff, H.; Burgess, R.; Choularton, T.; Gallagher, M. Studies of Heterogeneous Freezing by Three Different Desert Dust Samples. *Atmos. Chem. Phys.* **2009**, 9 (8), 2805–2824.
- (77) Weis, D. D.; Ewing, G. E. Water Content and Morphology of Sodium Chloride Aerosol Particles. *J. Geophys. Res. Atmos.* **1999**, *104* (D17), 21275–21285.
- (78) Sjogren, S.; Gysel, M.; Weingartner, E.; Baltensperger, U.; Cubison, M. J.; Coe, H.; Zardini, A. A.; Marcolli, C.; Krieger, U. K.; Peter, T. Hygroscopic Growth and Water Uptake Kinetics of Two-Phase Aerosol Particles Consisting of Ammonium Sulfate, Adipic and Humic Acid Mixtures. *J. Aerosol Sci.* 2007, 38 (2), 157–171.
- (79) Cziczo, D. J.; Abbatt, J. P. D. Infrared Observations of the Response of NaCl, MgCl₂, NH₄HSO₄, and NH₄NO₃ Aerosols to Changes in Relative Humidity from 298 to 238 K. J. Phys. Chem. A **2000**, 104 (10), 2038–2047.
- (80) Patnaude, R.; Diao, M.; Liu, X.; Chu, S. Effects of Thermodynamics, Dynamics and Aerosols on Cirrus Clouds Based on In Situ Observations and NCAR CAM6Model. *Atmos. Chem. Phys.* **2021**, *21* (3), 1835–1859.
- (81) Sassen, K.; Wang, Z.; Liu, D. Global Distribution of Cirrus Clouds from CloudSat/Cloud-Aerosol Lidar and Infrared Pathfinder Satellite Observations (CALIPSO) Measurements. *J. Geophys. Res.* **2008**, *113* (D8), D00A12.
- (82) Gasparini, B.; Meyer, A.; Neubauer, D.; Münch, S.; Lohmann, U. Cirrus Cloud Properties as Seen by the CALIPSO Satellite and ECHAM-HAM Global Climate Model. *J. Clim.* **2018**, *31* (5), 1983–2003.
- (83) Wernli, H.; Boettcher, M.; Joos, H.; Miltenberger, A. K.; Spichtinger, P. A Trajectory-Based Classification of ERA-Interim Ice Clouds in the Region of the North Atlantic Storm Track. *Geophys. Res. Lett.* **2016**, 43 (12), 6657–6664.
- (84) Liu, S.; Liu, C. C.; Froyd, K. D.; Schill, G. P.; Murphy, D. M.; Bui, T. P.; Dean-Day, J. M.; Weinzierl, B.; Dollner, M.; Diskin, G. S.; Chen, G.; Gao, R. S. Sea Spray Aerosol Concentration Modulated by Sea Surface Temperature. *Proc. Natl. Acad. Sci. U. S. A.* **2021**, *118* (9), e2020583118.